NRC Publications Archive
Archives des publications du CNRC

Design of thin InGaAsN(Sb) n - i - p junctions for use in four-junction concentrating photovoltaic devices
Wilkins, Matthew M.; Gupta, James; Jaouad, Abdelatif; Bouzazi, Boussairi; Fafard, Simon; Boucherif, Abderraouf; Valdivia, Christopher E.; Arès, Richard; Aimez, Vincent; Schriemer, Henry P.; Hinzer, Karin

National Research Council Canada   Conseil national de recherches Canada

Canada

Design of thin InGaAsN(Sb) *n-i-p* junctions for use in four-junction concentrating photovoltaic devices

Matthew M. Wilkins
James Gupta
Abdelatif Jaouad
Boussairi Bouzazi
Simon Fafard
Abderraouf Boucherif
Christopher E. Valdivia
Richard Arès
Vincent Aimez
Henry P. Schriemer
Karin Hinzer

SPIE.

Design of thin InGaAsN(Sb) *n-i-p* junctions for use in four-junction concentrating photovoltaic devices

Matthew M. Wilkins,[a] James Gupta,[b] Abdelatif Jaouad,[c,d]
Boussairi Bouzazi,[c,d] Simon Fafard,[c,d] Abderraouf Boucherif,[c,d]
Christopher E. Valdivia,[a] Richard Arès,[c,d] Vincent Aimez,[c,d]
Henry P. Schriemer,[a] and Karin Hinzer[a],*

[a]School of Electrical Engineering and Computer Science at the University of Ottawa,
25 Templeton Street, Ottawa K1N6N5, Canada
[b]Institute for Microstructural Sciences, National Research Council, 1200 Montreal Road,
Building M-50, Ottawa K1A 0R6, Canada
[c]Laboratoire Nanotechnologies Nanosystèmes (LN2), CNRS UMI-3463, 3000 Boulevard
Université, Sherbrooke J1K 0A5, Canada
[d]Université de Sherbrooke, Institut Interdisciplinaire d'Innovation Technologique (3IT),
3000 Boulevard Université, Sherbrooke J1K 0A5, Canada

Abstract. Four-junction solar cells for space and terrestrial applications require a junction with a band gap of ∼1 eV for optimal performance. InGaAsN or InGaAsN(Sb) dilute nitride junctions have been demonstrated for this purpose, but in achieving the 14 mA/cm^2 short-circuit current needed to match typical GaInP and GaAs junctions, the open-circuit voltage (V_{OC}) and fill factor of these junctions are compromised. In multijunction devices incorporating materials with short diffusion lengths, we study the use of thin junctions to minimize sensitivity to varying material quality and ensure adequate transmission into lower junctions. An *n-i-p* device with 0.65-μm absorber thickness has sufficient short-circuit current, however, it relies less heavily on field-aided collection than a device with a 1-μm absorber. Our standard cell fabrication process, which includes a rapid thermal anneal of the contacts, yields a significant improvement in diffusion length and device performance. By optimizing a four-junction cell around a smaller 1-sun short-circuit current of 12.5 mA/cm^2, we produced an InGaAsN(Sb) junction with open-circuit voltage of 0.44 V at 1000 suns (1 sun = 100 mW/cm^2), diode ideality factor of 1.4, and sufficient light transmission to allow >12.5 mA/cm^2 in all four subcells. © *2017 Society of Photo-Optical Instrumentation Engineers (SPIE)* [DOI: 10.1117/1.JPE.7.022502]

1 Introduction

Multijunction solar cells achieve the highest power conversion efficiency of any solar power technology as a result of their improved harvesting of the solar spectrum by absorbing different wavelengths in different p–n junctions called subcells. Three-junction lattice matched solar cells grown by molecular beam epitaxy (MBE) and incorporating a ∼1 eV dilute nitride subcell have shown excellent power conversion efficiency, including a result of 44.0% under 942 suns concentration[1,2] and 29% at 1 sun.[3] "Nonlattice matched" approaches using wafer bonding, metamorphic composition-graded buffers, and/or epitaxial liftoff have shown the greatest efficiency overall with successful four-junction devices reaching up to 46.0% under concentration using a wafer bonded architecture,[4,5] and 45.7% using an inverted metamorphic architecture.[6] In

---

contrast, a "lattice-matched" four-junction cell could yield near-record efficiency while avoiding the added costs associated with those techniques.

Previous numerical modeling studies on lattice-matched four-junction $Ga_{0.5}In_{0.5}P/Al_{0.05}GaAs/InGaAsN(Sb)/Ge$ cells incorporating dilute nitrides highlighted the importance of using photons efficiently, absorbing only those photons that have a high probability of being collected.[7] Hence, photons at wavelengths that cannot be collected efficiently are best used by transmitting through to the bottom germanium junction. In general, the lower junctions should have a slightly higher J_{SC} than the upper junctions in order to preserve the fill factor and efficiency of the multijunction device.[8] Due to the short diffusion length in InGaAsN(Sb), an *n-i-p* structure is commonly used to enhance carrier collection and provide an effective "collection length," which is longer than the diffusion length; furthermore, thick *n-i-p* InGaAsN(Sb) and InGaAsN(Bi) junctions are highly sensitive to background doping levels, and those doping levels are strongly dependent on annealing conditions.[9,10] In some cases, annealing can convert the background doping from *p*-type to *n*-type, causing the *p*-n junction to be located at the back of the absorber and reducing the quantum efficiency.[9] Consequently, these subcells with materials having lower mobilities must be carefully considered within the context of operating characteristics of the complete device.

In this article, we present an experimental study of dilute nitride InGaAsN(Sb) junction designs to be incorporated in four-junction solar cells. To that end, the design of the InGaAsN(Sb) subcell is optimized for concentrating photovoltaic applications, and the surrounding layers are designed to replicate the optical environment of a $Ga_{0.5}In_{0.5}P/Al_{0.05}GaAs/InGaAsN(Sb)/Ge$ device. A filter layer is included to block light that would be absorbed in the top two junctions, with its material and thickness chosen to match that of the second junction of our hypothetical four-junction structure. We use a relatively thin InGaAsN(Sb) junction to make it more robust with respect to varying material quality. This thin junction avoids negatively impacting the performance of other junctions, is current-matched to a fully lattice matched four-junction cell, and could be easily adapted for devices of five junctions or more.

2 Methods

Following the design study that was conducted in simulation,[11,12] a nominal design (D1) and two variants (D2 and D3) were prepared to cover the design space that would provide adequate short-circuit current density with minimal collection losses. In the D1 design, a nominally intrinsic InGaAsN(Sb) absorber layer of 1.0-μm thickness was used, similar to many previous works on InGaAsN(Sb) cells.[4,13] D2 is identical except for the use of a thinner absorber of 0.65-μm

Table 1 Layer structures of the three designs. Differences are in bold face.

Layer	Material	D1 Doping (cm^{-3})	D1 Thickness (μm)	D2 Doping (cm^{-3})	D2 Thickness (μm)	D3 Doping (cm^{-3})	D3 Thickness (μm)
Cap	GaAs			$n\, 5 \times 10^{18}$	0.05		
Filter	Al$_{0.05}$Ga$_{0.95}$As			$n\, 1 \times 10^{18}$	2.00		
Window	Al$_{0.5}$Ga$_{0.5}$As			$n\, 5 \times 10^{18}$	0.05		
n-Emitter	GaAs			$n\, 5 \times 10^{18}$	0.05		
Absorber	InGaAsN(Sb)	***I***	**1.00**	***i***	**0.65**	***p*** $\mathbf{1 \times 10^{16}}$	**0.65**
p-Base	GaAs			$p\, 1 \times 10^{19}$	0.05		
Sacrif.	InGaAsN(Sb)	***p*** $\mathbf{1 \times 10^{17}}$	**0.20**	***p*** $\mathbf{1 \times 10^{17}}$	**0.20**	**layer omitted**	
Buffer	GaAs			$p\, 1 \times 10^{18}$	0.20		
Substr.	GaAs			p	650		

thickness, as listed in Table [1]. Both D1 and D2 include a 0.2-μm sacrificial dilute nitride layer to incorporate any pre-existing surface impurities, as suggested by Ptak.[14] As an added benefit, this layer helps to replicate operating conditions in the middle of a four-junction device with a germanium bottom junction by absorbing some of the light which might otherwise be reflected from the back surface of the wafer and be absorbed on a second pass through the InGaAsN(Sb) junction.

The D3 design also included a thin 0.65-μm absorber, which was intentionally *p*-doped to 1×10^{16} cm^{-3}, but the sacrificial layer was omitted. Given that InGaAsN(Sb) material can often have n-type background doping, this ensures that we have a p-type cell, with the junction near the front to compare against. For each design, a simulated cross-sectional band diagram is shown in Fig. [1]. These are calculated using drift-diffusion based simulations which have been described in Refs. [11] and [12].

Three wafers (one wafer of each design) were grown by MBE in a custom V90 system containing valved cracker sources for As$_2$ and Sb$_2$ and conventional effusion cells for the group-III elements and dopants. Active nitrogen was provided by a radio frequency plasma source using N$_2$/Ar dynamic gas switching. Details of the growth method can be found in Refs. [15] and [16]. Biased deflector plates, such as those used in Ref. [13], were not employed here. The growths were performed on 76-mm diameter, single-side polished Zn-doped GaAs substrates with $(100) \pm 0.1$ deg orientation.

We prepared samples of each design using a complete fabrication process. Photolithography was used to define the contact patterns with a positive resist. The grid lines and busbar regions were protected by the photoresist and the GaAs cap layer was etched selectively relative to the window layer in an NH$_4$OH:H$_2$O$_2$:H$_2$O solution. The photoresist was stripped and the sample was cleaned. The surface was deoxidized using a buffered hydrofluoric acid solution and the
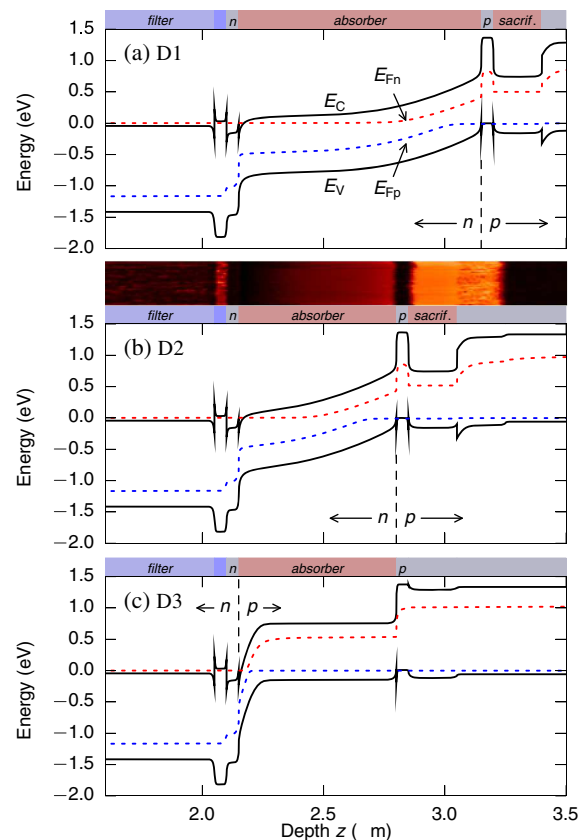
Fig. 1 Simulated energy band diagrams of (a) D1, (b) D2, and (c) D3 at short circuit with 1000 suns illumination, AM1.5D spectrum. In (b), the scanning probe microscope tip-sample resistance, as measured with SSRM, is also shown as a function of position; brighter color indicates higher resistance. Scanning probe measurements were done with all device layers grounded.

samples were immediately introduced into a plasma-enhanced chemical vapour deposition reactor. A second photolithography process using double resist layers was performed, followed by a standard deposition/lift-off process to define the ohmic contact (a Ni/Ge/Au/Ni metal structure prepared by e-beam evaporation). The backside contact was obtained by e-beam evaporation of Ti/Pt/Au. The contacts were annealed for 1 min at 430°C in a forming gas atmosphere. A thick contact layer of Ti/Au (20 nm/4000 nm) was evaporated on the back side, including grid deposition and rapid thermal anneal. The GaAs cap layer was removed by etching, but no antireflective coating was applied.

3 Results

3.1 *Carrier Collection*

A study of an unannealed D2 wafer sample using cross-sectional scanning capacitance microscopy indicated that the undoped material in these devices is *n*-type. This was confirmed by scanning spreading resistance microscopy (SSRM). SSRM results are incorporated in Fig. 1(b), with brighter colors indicating higher resistance, and show that the material resistivity increases toward the back side of the InGaAsN(Sb) layer, hence, the material is most depleted of carriers near that interface. The presence of a gradient in resistivity throughout the width of the InGaAsN(Sb) absorber indicates that there is significant depletion resulting from a strong built-in electric field over the full thickness of the absorber. Our device simulations show a similar gradient in resistivity when an *n*-type background doping of 2×10^{15} cm^{-3} is used.

External quantum efficiency (EQE) of the devices was measured with a Newport IQE-200 system. Specular and diffuse reflectivity, R_s and R_d, were also measured and used to calculate internal quantum efficiency (IQE) according to IQE = EQE/$(1 - R_s - R_d)$.

In Fig. 2, all samples show a steady reduction in IQE for longer wavelengths, which is expected due to the optically thin absorber. The samples show an absorption edge at 1400 nm, consistent with an effective InGaAsN(Sb) band gap of 0.90 eV. Although the AM1.5D solar spectrum provides little photon flux in the 1300- to 1400-nm range due to a water absorption line, there is still an advantage to this low band gap material in that its absorption coefficient at the relevant wavelengths of 830 to 1300 nm is increased as compared to a 1.0 eV design. Data on the near-bandgap absorption coefficient of dilute nitride materials were reported by Kurtz et al.[7]
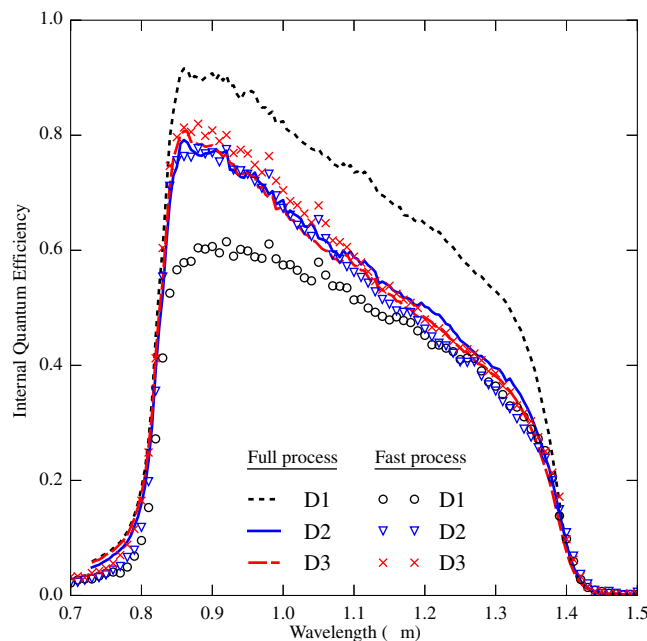
Fig. 2 IQE of the full-process and fast-process samples.

All of the IQE measurements show a small tail extending to photon energies well above the $Al_{0.05}Ga_{0.95}As$ band gap at 830 nm. This could be a result of luminescent coupling from the AlGaAs filter into the InGaAsN(Sb) absorber[17] and will not necessarily contribute photocurrent in an operating four-junction device, unless the junctions with larger band gaps are producing an excess of photocurrent.[18]

To characterize the InGaAsN(Sb) junctions in a nearly as-grown condition with minimal annealing, a set of "fast-process" samples were prepared from 5 mm × 5 mm dies cleaved from the as-grown wafer. These samples were prepared with ohmic indium contacts to the top and bottom faces and are sufficient for quantum efficiency measurements, but the contacts are not adequate for operation at high currents. The advantage of this process is that the contacts are formed with only a 30 s anneal at 200°C, which we consider to be negligible in terms of its effect on the dilute nitride material.

The cap layer was not etched away for these experiments; we estimate that the cap parasitically absorbs 0.14 mA/cm^2 of the available 1-sun photocurrent, based on simulated IQE with and without the cap layer.

EQE and IQE of these samples were measured using a four-wire connection to the device under test. The illuminating 2 mm × 0.5 mm beam was positioned such that it was not incident on the top contacts. The "fast-process" D1 samples with the 1.0-μm absorber have the lowest peak IQE, at 60%, and short-circuit current density, J_{SC} of 13.4 mA/cm^2, calculated using the IQE with reference to the AM1.5D spectrum at 100 mW/cm^2 (1 sun). These are the only samples which show significant improvement under reverse bias, where the peak IQE increases by 17% absolute at −1 V; minimal further improvement was found for larger biases. The D2 and D3 samples with the 0.65-μm thick absorber reach a peak IQE of 75% and 81%, respectively, with J_{SC} of 15.0 and 16.6 mA/cm^2, respectively. Despite the thinner absorber, these samples show higher IQE overall, and the absence of any uncollected absorption is a benefit for integration in a multijunction device, where any transmitted light may be absorbed in the next junction. The difference between the 0.65- and 1.0-μm absorbers is most pronounced at short wavelengths, which are absorbed toward the top of the junction. Given that the absorber is most heavily depleted toward the bottom of the layer due to *n*-type background doping, it is likely that the built-in electric field is insufficient to collect carriers from the front of the thick 1.0-μm, fast-process absorber [Fig. 1(a)].

The InGaAsN(Sb) subcell was designed based on the results of simulations of complete four-junction structures, with the intention of having an overall J_{SC} of 12.5 mA/cm^2 for the four-junction device. Both the InGaAsN(Sb) junction and the Ge junction are intended to have J_{SC} exceeding 12.5 mA/cm^2 in order to maintain a high fill factor.[9] We have achieved this in the InGaAsN(Sb) junction, and the measured QE is consistent with our simulations, which indicate ~13 mA/cm^2 in the Ge subcell when the 0.65-μm absorber is used. The 1-μm absorber would absorb too much, thus in that case, the 4J device would be limited by the bottom germanium subcell with a J_{SC} of ~8.3 mA/cm^2.

Comparing the "fast process" and fully fabricated D1 samples, we observed a change in peak IQE from 60% to 90%, yielding a 35% improvement in J_{SC}. The thinner D2 and D3 samples showed no change with processing, and IQE is consistent with full collection of generated carriers. These observations are consistent with a collection length (combining the effects of drift and diffusion) of at least 0.65 μm in all of the fast-processed samples, which improved to >1 μm in the fully fabricated samples. The increased collection length could be caused by either improved diffusion length, a change in background doping type, or a wider depletion region within the dilute nitride absorber. SSRM measurements of the full-process D1 sample show no significant changes in the resistivity profile through the sample as would be expected for the latter two possibilities, thus a change in diffusion length is indicated. We find good agreement between simulations and measurement with a "diffusion" length of 0.3 μm before annealing and >1.0 μm after annealing.

3.2 *Current–Voltage Characterization*

When integrated in a four-junction solar cell, we estimate that the complete cell would operate with $J_{SC} \sim 12.5$ mA/cm^2 and maximum-power current density $J_{MP} \sim 11.5$ mA/cm^2 under 1-sun, AM1.5D conditions, based on our previous study of photocurrent sharing between
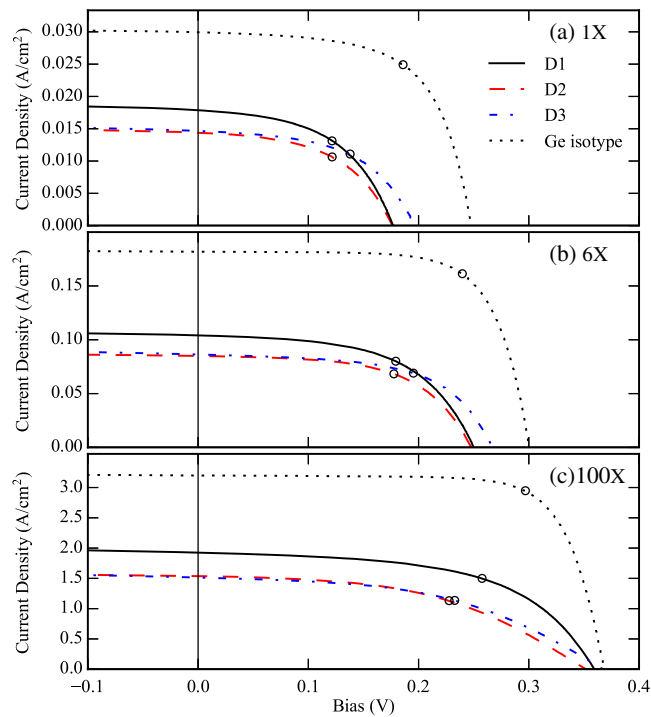
Fig. 3 $J - V$ curves of the fabricated devices at concentrations of (a) 1, (b) 6, and (c) 100 suns. The concentration is as indicated by a GaInP/GaAs/Ge reference cell; no mismatch correction has been applied. Maximum power points are indicated with black circles.

the four junctions.[12] Therefore, it is important that similar current density is available from the InGaAsN(Sb) subcell; in fact, it is advantageous for the InGaAsN(Sb) cell to overproduce somewhat relative to the higher junctions so that it will not have a negative impact on fill factor of the multijunction device.[8,12] Current densities (J) were measured across a range of bias voltages (V) at concentrations of 1, 6, and 100 suns using an Alpha-Omega Power Technologies xenon flash solar simulator. The results are shown in Fig. 3. For the 0.65-μm designs D2 and D3, we find little difference in performance despite D3 being intentionally doped and having minimal electric field in the absorber [see Fig. 1(c)], indicating that the drift-aided collection may not be important at this absorber thickness. All three designs show a significant reduction in the slope near V_{OC}, which we consider to be a parasitic resistance.

We next consider the performance of the cells under high concentration. *n-i-p* junctions rely on the built-in electric field to drive carriers across the junction, but this field is reduced when the cell is operating under voltage bias. Therefore, many *n-i-p* structures show a reduction in collected photocurrent as bias increases,[13–15] and hence a reduction in fill factor and V_{OC}. This is evident as a small slope in the $J - V$ curves near J_{SC}, which is present at all concentrations. In contrast, a shunt conductance would lead to a similar slope but would have reduced impact as concentration increases.

We also see significant effects due to series resistance, which reduce fill factor and efficiency at 100 suns [Fig. 3(c)]. Consequently, we find that 6× is the maximum practical concentration for these samples. We expect that the impact of series resistance, and to a lesser extent the bias-dependent carrier collection, can be reduced in an optimized device as has been demonstrated in the literature.[8]

For the lower concentration measurements described above, V_{OC} values were extracted from the individual $J - V$ curves. The top contacts were not optimized for large currents and so for the higher concentrations, on the order of 1000 suns, V_{OC} values were determined explicitly by testing at open circuit. All of the measured V_{OC} values are plotted in Fig. 4 against concentration, which has been corrected for spectral mismatch to AM1.5D,[12] in order to extract the diode ideality factors n for the various designs. The Ge isotype demonstrates $n = 1$ behavior, but the three *n-i-p* designs show $n = 1.4$ behavior up to the maximum measured intensity of 1500 suns,
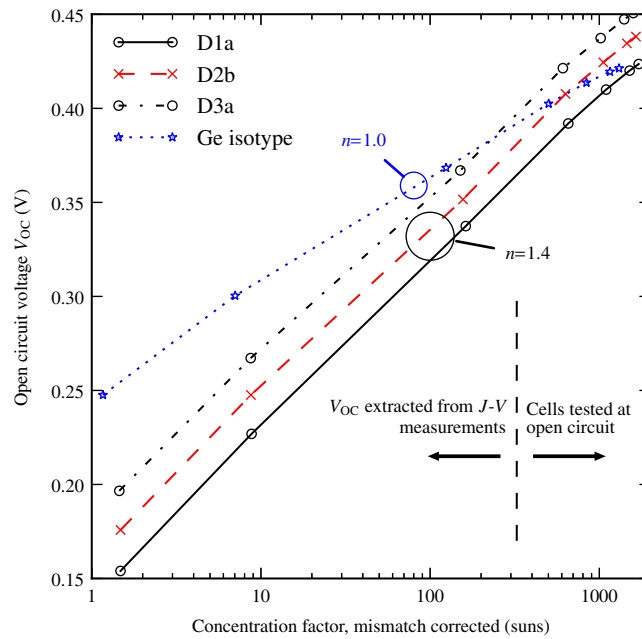
Fig. 4 Open-circuit voltage as a function of concentration for the three designs under a xenon flash solar simulator, where 1 sun = 100 mW/cm^2.

Table 2 Measured parameters of the fully fabricated devices. J_{SC} is calculated by integrating the measured IQE with the AM1.5D spectrum scaled to 100 mW/cm^2.

Device	J_{SC} (mA/cm^2)	1-sun V_{OC} (V)	1000-sun V_{OC} (V)
D1	18.5	0.166	0.428
D2	15.1	0.164	0.422
D3	14.4	0.186	0.436

indicating that V_{OC} is significantly influenced by recombination in the wide space charge region, at least up to the maximum measured bias of 0.45 V.

Table 2 summarizes J_{SC} and V_{OC} of the fully fabricated devices for reference. To illustrate what may be achieved with finished devices, which would have appropriate antireflection coatings, J_{SC} values are reported as the integral of device IQE with the reference spectrum, rather than extracted from the $J - V$ curves. All of the J_{SC} values are adequate to exceed the expected four-junction J_{SC} of 12.5 mA/cm^2. Simulations show that these results are consistent with ~100% collection of carriers that are generated in the InGaAsN(Sb) absorber. D1 somewhat exceeds the needed current density and if this material quality can be achieved consistently, the design could be adapted to use a larger band gap of 0.95 eV. At this point though, we do not have consistent results from sample to sample with the D1 design, whereas D2 and D3 are more robust to changes in processing.

Using the 1-sun V_{OC}, the band gap-voltage offsets $W_{OC} = qE_g - V_{OC,1-sun}$ are 0.76, 0.74, and 0.71 V for the D1, D2, and D3 designs, respectively. For reference, an offset of 0.4 V is usually considered to be an indication of "good quality" material. These values are, however, in line with some other reported InGaAsN(Sb) devices[7] and InGaAsN(Bi) devices.[10] More recently, Miyashita et al.[2] have shown InGaAsN(Sb) solar cells with W_{OC} as low as 0.58 V. As concentration increases, V_{OC} of the InGaAsN(Sb) devices surpasses that of our 0.67 eV Ge isotype at ~300 to 1000 suns. The D3 sample which had the lowest J_{SC} has the greatest V_{OC}. V_{OC} and fill factor will need to be improved further in order for a four-junction device to reach a competitive level of efficiency. In particular, the apparent series resistance of these samples prevents them from being used at high concentration.

If we take our previous simulations of four-junction cells under 1000-sun AM1.5D illumination and substitute InGaAsN(Sb) junctions with the measured J_{SC}, V_{OC}, and ideality factor, as listed in Table 2 (but with no series resistance), we find efficiencies of 29.7%, 42.9%, and 43.1% for D1, D2, and D3, respectively. The D1 efficiency is low, as expected, due to its optically thick absorber layer, which passes insufficient light through to the bottom junction.

4 Conclusion

In summary, we have presented results of InGaAsN(Sb) cells, which exceed the 12.5 mA/cm^2 at 1-sun needed for current matching in a four-junction, GaInP/(Al)GaAs/InGaAsN(Sb)/Ge solar cell. The cells have minimal collection losses; photons that are not collected as carriers will be transmitted through to the next lower subcell rather than being lost. The 0.65-μm design is robust against changes in background doping and annealing condition, which is promising for integration into a full multijunction device. A similar design approach may be applicable to other devices, such as lattice matched, InGaAsN(Sb)-based multiband photodetectors.

Acknowledgments

References

1. J. Allen et al., "44%-efficiency triple-junction solar cells," in *9th Int. Conf. on Photovoltaic Systems (CPV-9)*, Miyazaki, Japan (2013).
2. V. Sabnis, H. Yuen, and M. Wiemer, "High-efficiency multijunction solar cells employing dilute nitrides," in *8th Int. Conf. on Concentrating Photovoltaic Systems, AIP Conf. Proc.*, Vol. 1477, pp. 14–19 (2012).
3. A. Tukiainen et al., "High-efficiency GaInP/GaAs/GaInNAs solar cells grown by combined MBE-MOCVD technique," *Prog. Photovoltaics Res. Appl.* **24**, 914–919 (2016).
4. M. A. Green et al., "Solar cell efficiency tables (version 48)," *Prog. Photovoltaics Res. Appl.* **24**, 905–913 (2016).
5. F. Dimroth et al., "Four-junction wafer-bonded concentrator solar cells," *IEEE J. Photovoltaics* **6**(1), 343–349 (2016).
6. R. M. France et al., "Design flexibility of ultra-high efficiency 4-junction inverted metamorphic solar cells," in *2015 IEEE 42nd Photovoltaic Specialist Conf. (PVSC)*, pp. 1–3 (2015).
7. M. Wilkins et al., "Design constraints of *n-p* InGaAsN dilute nitride sub-cells for 3- and 4- junction solar cell applications under concentrated illumination," in *Proc. of the 39th IEEE Photovoltaics Specialists Conf.*, Tampa (2013).
8. G. Arbez et al., "4 junction dilute nitride solar cell optimization: comparing current matching approaches in detailed balance algorithms," in *Proc. of the 39th Photovoltaic Specialists Conf.*, Tampa, Florida (2013).
9. S. Kurtz et al., "Effects of in situ annealing on GaInNAs Solar cells," in *Proc. of the 39th Photovoltaic Specialists Conf.* (2013).
10. A. J. Ptak et al., "Effects of bismuth on wide-depletion-width GaInNAs solar cells," *J. Vac. Sci. Technol. B* **26**(3), 1053–1057 (2008).
11. M. Wilkins et al., "Effects of luminescent coupling in single- and 4-junction dilute nitride solar cells," in *Proc. of the 40th Photovoltaic Specialists Conf.*, Denver, Colorado, pp. 6–9 (2014).
12. M. M. Wilkins et al., "4-junction solar cells with dilute nitrides: optimization with luminescent coupling," in *Proc. of the 29th EU PVSEC*, Amsterdam, Netherlands (2014).
13. D. B. Jackrel et al., "Dilute nitride GaInNAs and GaInNAsSb solar cells by molecular beam epitaxy," *J. Appl. Phys.* **101**(11), 114916 (2007).

14. A. J. Ptak et al., "Calcium impurities in enhanced-depletion-width GaInNAs grown by molecular-beam epitaxy," *J. Vac. Sci. Technol. B* **24**(3), 1540 (2006).
15. J. A. Gupta et al., "Compositional control in molecular beam epitaxy growth of GaN_yAs_{1-y} on GaAs (001) using an Ar/N_2 RF plasma," *J. Cryst. Growth* **242**, 141–154 (2002).
16. J. A. Gupta et al., "Molecular beam epitaxy growth of GaInNAs(Sb) double quantum wells with bright and narrow photoluminescence," *J. Cryst. Growth* **291**, 86–93 (2006).
17. S. Kurtz et al., "Modeling of electron diffusion length in GaInAsN solar cells," in *Conf. Record of the Twenty-Eighth IEEE Photovoltaic Specialists Conf.*, pp. 1210–1213 (2000).
18. D. Derkacs, D. T. Bilir, and V. A. Sabnis, "Luminescent coupling in GaAs/GaInNAsSb multijunction solar cells," *IEEE J. Photovoltaics* **3**(1), 520–527 (2013).
19. J. Nelson, *Physics of Solar Cells*, Imperial College Press, London, United Kingdom (2003).
20. M. Wolf, "Drift fields in photovoltaic solar energy converter cells," *Proc. IEEE* **51**(5), 674–693 (1963).
21. D. J. Friedman and S. R. Kurtz, "Breakeven criteria for the GaInNAs junction in GaInP/ GaAs/GaInNAs/Ge four-junction solar cells," *Prog. Photovoltaics Res. Appl.* **10**, 331–344 (2002).
22. K. Emery et al., "Procedures for evaluating multijunction concentrators," in *Conf. Record of the Twenty-Eighth IEEE Photovoltaic Specialists Conf.*, pp. 1126–1130, IEEE (2000).
23. A. J. Ptak, D. J. Friedman, and S. Kurtz, "Effects of temperature, nitrogen ions, and antimony on wide depletion width GaInNAs," *J. Vac. Sci. Technol. B* **25**(3), 955 (2007).
24. N. Miyashita, N. Ahsan, and Y. Okada, "Generation and collection of photocarriers in dilute nitride GaInNAsSb solar cells," *Prog. Photovoltaics Res. Appl.* **24**, 28–37 (2016).

Matthew Wilkins received his MSc degree in systems science from the University of Ottawa in 2013, and he is currently a PhD candidate in electrical engineering. He previously worked for two companies doing research in renewable energy technologies. He has coauthored over 38 journal articles and conference proceedings.

Karin Hinzer received her PhD in physics from the University of Ottawa, Canada, in 2002. She is a Tier II Canada research chair in Photonic Nanostructures and Integrated Devices and an associate professor at the School of Electrical Engineering and Computer Science (EECS) at the University of Ottawa. She received the 2016 Young Researcher Award from uOttawa. She has coauthored over 135 peer-reviewed publications, including two landmark papers in science.

Biographies for the other authors are not available.